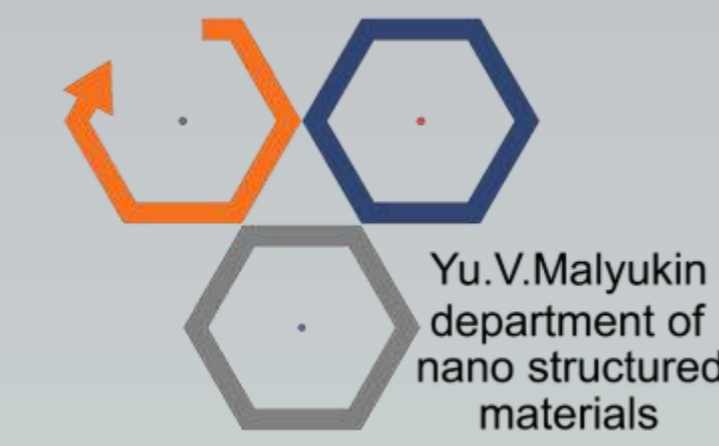


Simultaneous turn-off and ratiometric detection of HP using redox-active $\text{CeO}_{2-x}:\text{Eu}^{3+}$ colloidal nanosensors

Yevhen Neuhodov, Pavel Maksimchuk, Andrey Onishchenko, Nataliya Kavok, Galyna Dudetskaya, Yurii Kot, Svetlana Yefimova, Vladyslav Seminko

Yu. V. Malyukin Department of Nanostructured Materials, Institute for Scintillation Materials, NAS of Ukraine

e.i.neuhodov@gmail.com



Yu.V.Malyukin
department of
nano structured
materials

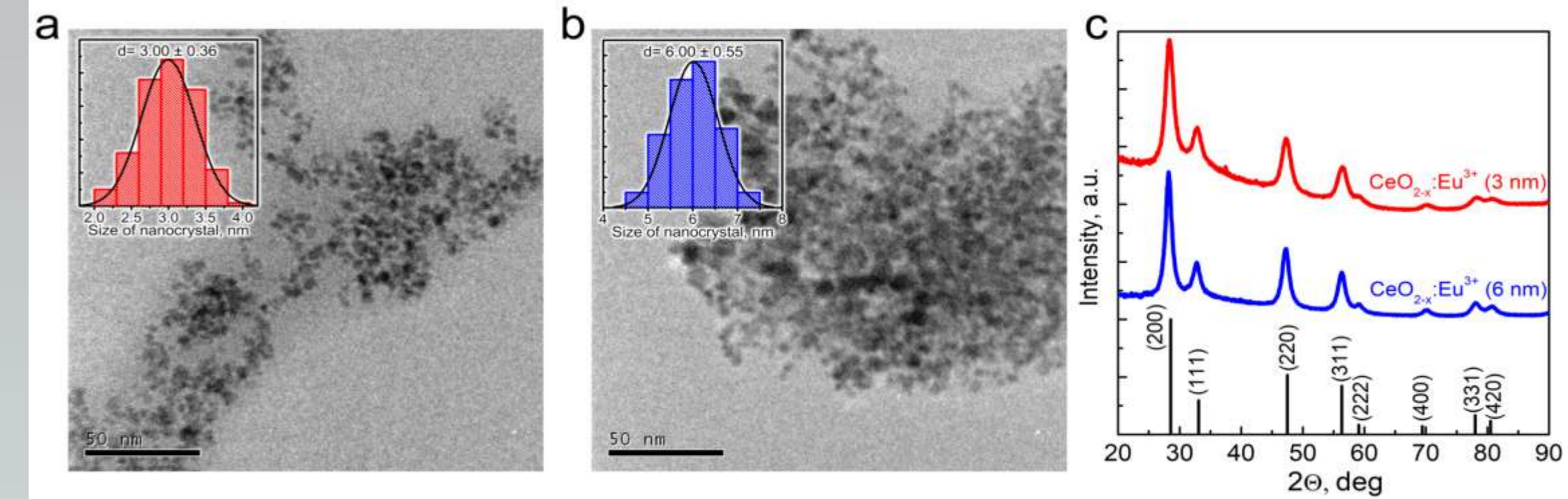


Fig. 1 TEM images of a) 3 nm and b) 6 nm $\text{CeO}_{2-x}:\text{Eu}^{3+}$ nanoparticles with size distributions shown in the insets, c) XRD of 3 nm and 6 nm $\text{CeO}_{2-x}:\text{Eu}^{3+}$ nanoparticles.

Abstract

Hydrogen peroxide (HP) is a central signaling molecule in physiological systems and a critical byproduct of enzymatic activities involving catalase and superoxide dismutase.

Despite the high sensitivity of traditional organic fluorescent probes, their practical application is often restricted by poor chemical stability, susceptibility to photobleaching, and a fundamental lack of reversibility.

To address these challenges, this study introduces ultra-small (3 nm and 6 nm) Eu^{3+} -doped colloidal ceria nanoparticles ($\text{CeO}_{2-x}:\text{Eu}^{3+}$) as a robust and stable inorganic alternative. These nanoparticles, synthesized via a controlled hydrolysis process, maintain a face-centered cubic structure and offer a unique multi-channel sensing platform that combines turn-off and ratiometric detection modes.

The operational logic of the $\text{CeO}_{2-x}:\text{Eu}^{3+}$ sensor is based on the complex interplay between surface redox reactions and luminescence properties. The turn-off channel utilizes the reversible quenching of Ce^{3+} (430 nm) and Eu^{3+} (591 nm) luminescence bands. Detailed statistical analysis demonstrates that this quenching does not follow the standard Stern-Volmer model but is instead governed by surface-adsorption mechanisms. Specifically, the Ce^{3+} band quenching aligns with the Temkin adsorption model, reflecting the energetic inhomogeneity of the nanoparticle surface, while the Eu^{3+} band follows a Langmuir-like behavior. Mechanistically, HP molecules adsorbed on the surface oxidize Ce^{3+} to Ce^{4+} , while the hydroxyl radicals produced during HP decomposition act as the primary quenchers for Eu^{3+} ions.

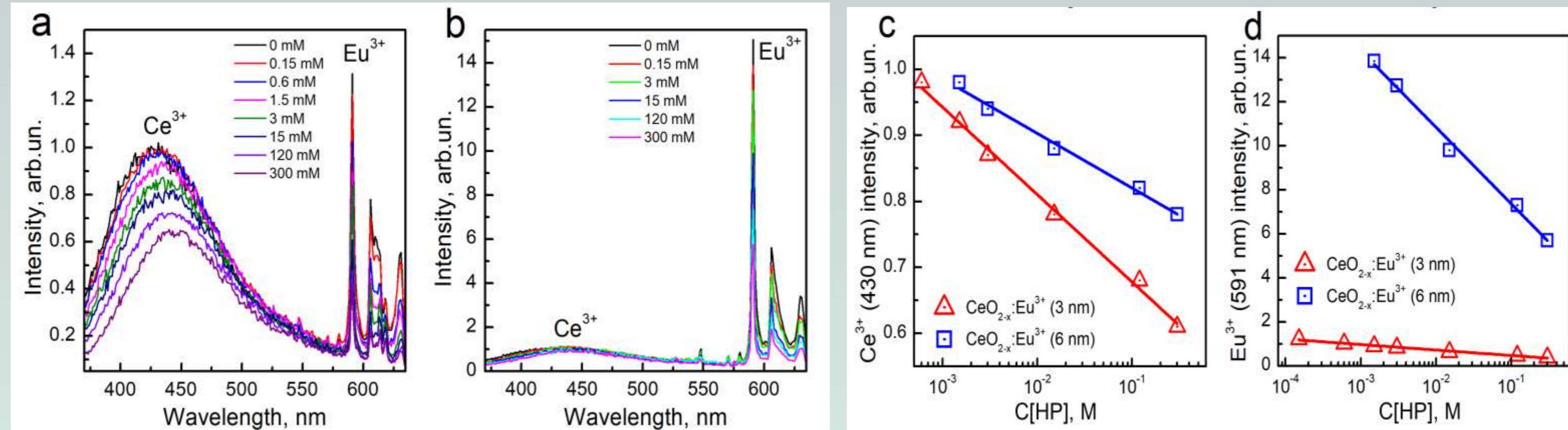


Fig. 2 The luminescence spectra of 3 nm (a) and 6 nm (b) $\text{CeO}_{2-x}:\text{Eu}^{3+}$ nanoparticles depending on HP concentrations in water solutions, and dependences of Ce^{3+} (430 nm) (c) and Eu^{3+} (591 nm) (d) luminescence intensities on HP concentration.

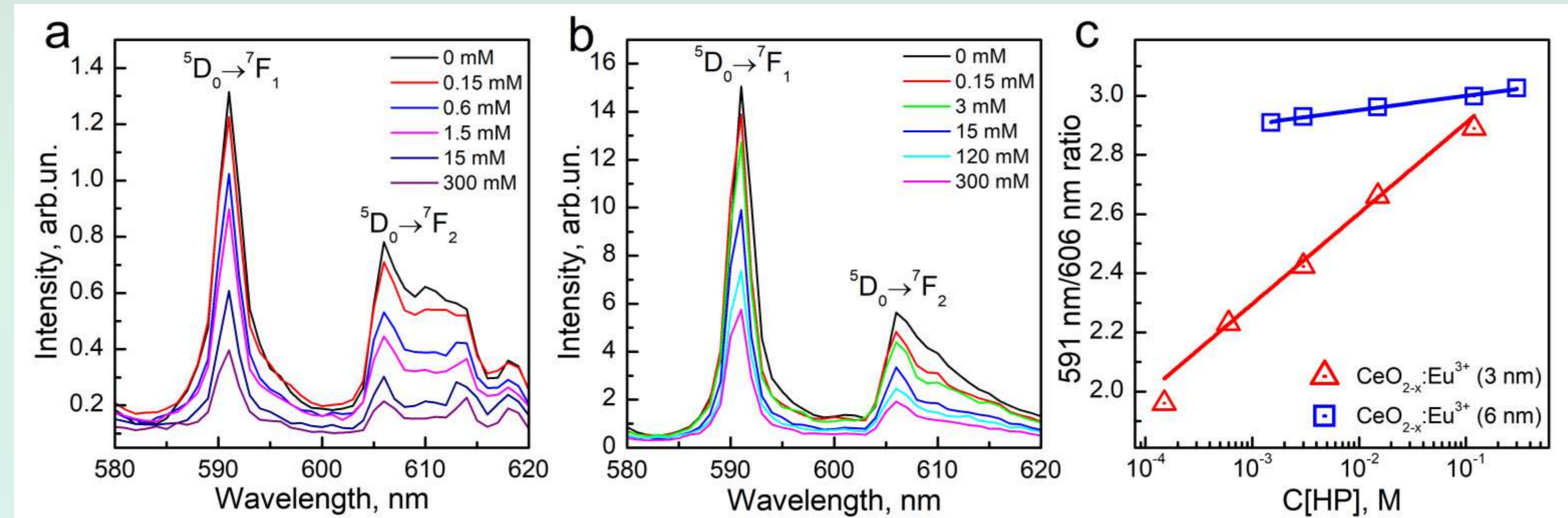


Fig. 3 The luminescence spectra of 3 nm (a) and 6 nm (b) $\text{CeO}_{2-x}:\text{Eu}^{3+}$ nanoparticles in the 585 nm - 620 nm spectral range depending on HP concentrations in water solutions, and dependence of the ratio of intensities of $^5\text{D}_0 \rightarrow ^7\text{F}_1$ and $^5\text{D}_0 \rightarrow ^7\text{F}_2$ Eu^{3+} luminescence bands on HP concentration (c).

Conclusion

Furthermore, the system provides a self-calibrating ratiometric signal based on the intensity ratio of Eu^{3+} transitions ($^5\text{D}_0 \rightarrow ^7\text{F}_1$ and $^5\text{D}_0 \rightarrow ^7\text{F}_2$). As HP-induced oxidation reduces the concentration of oxygen vacancies in the lattice, the local symmetry surrounding the Eu^{3+} ions increases, leading to a measurable shift in the 591/606 nm ratio. This ratiometric sensitivity is particularly pronounced in 3 nm nanoparticles due to their higher initial defect density.

Thus, $\text{CeO}_{2-x}:\text{Eu}^{3+}$ nanoparticles represent an effective inorganic platform for multi-channel hydrogen peroxide detection, providing high reliability through the combination of ratiometric and turn-off sensing modes.

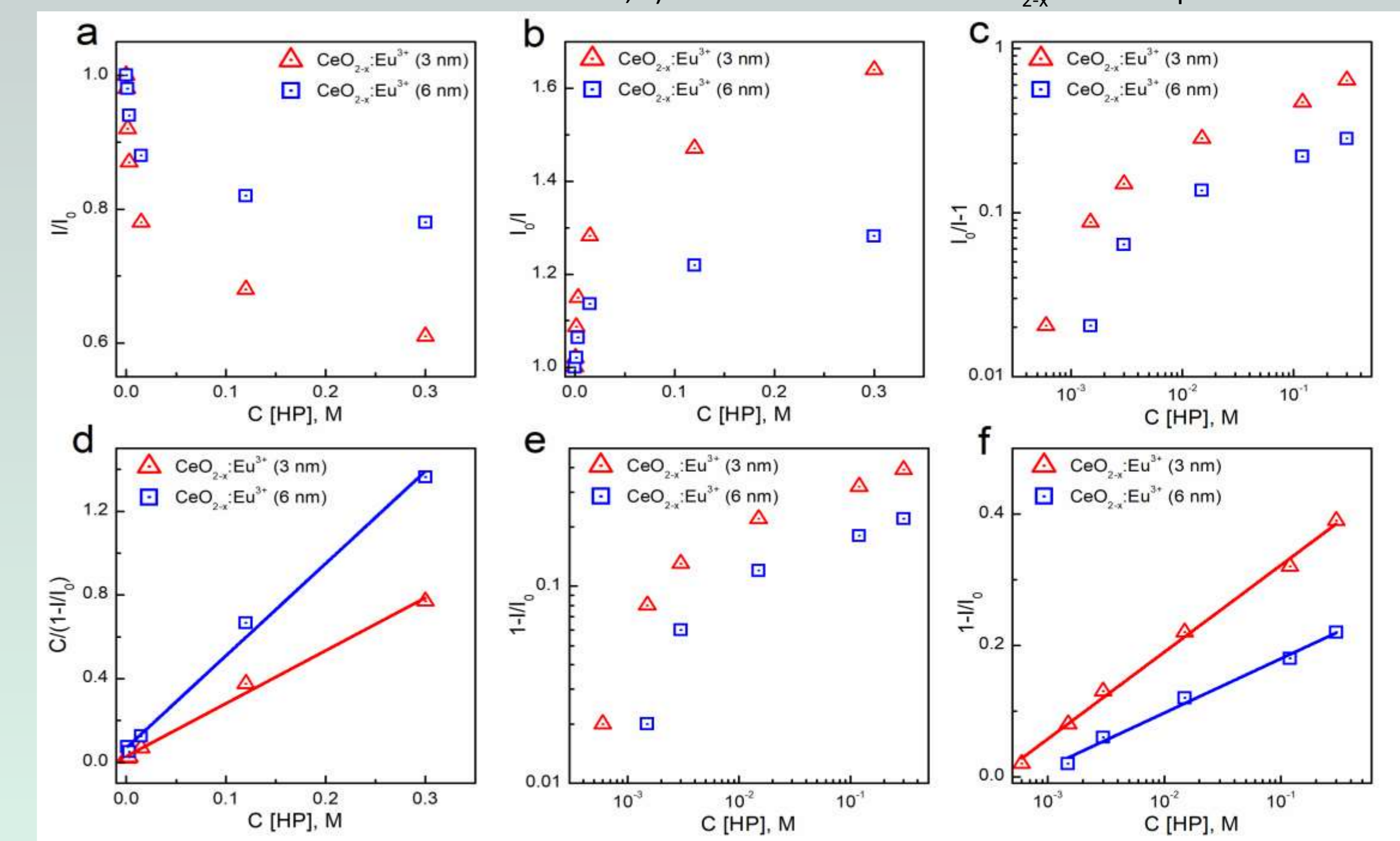


Fig. 4 The concentration dependences of Ce^{3+} luminescence intensity (430 nm) shown as is (a), on the I_0/I vs $C[\text{HP}]$ plot (Stern-Volmer model) (b), on the $\log(\Delta I/I)$ vs $\log C[\text{HP}]$ plot (modified Stern-Volmer model) (c), on the $C[\text{HP}]/(\Delta I/I_0)$ vs $C[\text{HP}]$ plot (Langmuir adsorption model) (d), on the $\log(1-I/I_0)$ vs $\log C[\text{HP}]$ plot (Freundlich adsorption model) (e), and on the $1-I/I_0$ vs $\log C[\text{HP}]$ plot (Temkin adsorption model) (f).

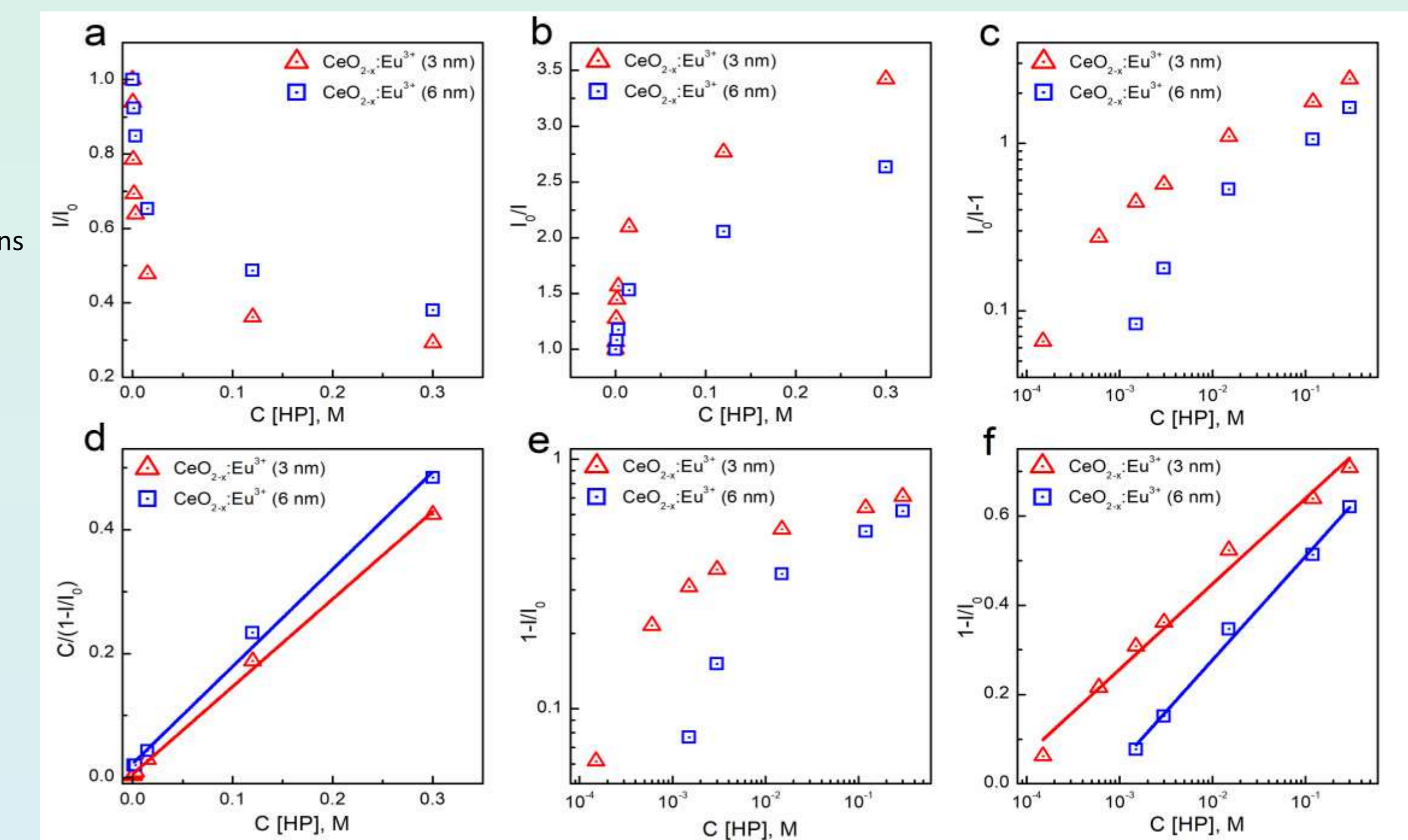


Fig. 5 The concentration dependences of Eu^{3+} luminescence intensity (591 nm) shown as is (a), on the I_0/I vs $C[\text{HP}]$ plot (Stern-Volmer model) (b), on the $\log(\Delta I/I)$ vs $\log C[\text{HP}]$ plot (modified Stern-Volmer model) (c), on the $C[\text{HP}]/(\Delta I/I_0)$ vs $C[\text{HP}]$ plot (Langmuir adsorption model) (d), on the $\log(1-I/I_0)$ vs $\log C[\text{HP}]$ plot (Freundlich adsorption model) (e), and on the $1-I/I_0$ vs $\log C[\text{HP}]$ plot (Temkin adsorption model) (f).

This research was supported by National Research Foundation of Ukraine, Grant № 2023.03/0050